Maize EHD1 is Required for Kernel Development and Vegetative Growth through Regulating Auxin Homeostasis

Yafei Wang[1,2], Wenwen Liu[2], Hongqiu Wang[1,2], Qingguo Du[2], Zhiyuan Fu[1], Wen-Xue Li[2,*] and Jihua Tang[1,*]

[1]National Key Laboratory of Wheat and Maize Crop Science, Collaborative Innovation Center of Henan Grain Crops, College of Agronomy, Henan Agricultural University, Zhengzhou, 450002, China;

[2]National Engineering Laboratory for Crop Molecular Breeding, Institute of Crop Science, Chinese Academy of Agricultural Sciences, Beijing 100081, China

[*]To whom correspondence should be addressed:

Jihua Tang

Tel: +86-371-63558377

E-mail: tangjihua1@163.com

Wen-Xue Li

Tel: +86-10-82105799

E-mail: liwenxue@caas.cn

Running title: ZmEHD1-mediated CME regulates maize auxin homeostasis

Abstract

The roles of EHDs in clathrin-mediated endocytosis (CME) in plants are poorly understood. Here, we isolated a maize mutant, designated as *ehd1*, which showed defects in kernel development and vegetative growth. Positional cloning and transgenic analysis revealed that *ehd1* encodes an EHD protein. Internalization of the endocytic tracer FM4-64 was significantly reduced in *ehd1* mutant and *ZmEHD1* knock-out mutants. We further demonstrated that ZmEHD1 and ZmAP2 σ subunit physically interact in the plasma membranes. Cellular IAA levels were significantly lower in *ehd1* mutant than in wild-type maize. Auxin distribution and ZmPIN1a-YFP localization were altered in *ehd1* mutant. Exogenous application of 1-NAA but not GA3 rescued the seed germination and seedling emergency phenotypic defects of *ehd1* mutants. Taken together, these results indicate that ZmEHD1 regulates auxin homeostasis by mediating CME through its interaction with the ZmAP2 σ subunit, which is crucial for kernel development and vegetative growth of maize.

Introduction

Endocytosis, which can be clathrin-dependent or clathrin-independent, is the internalization of plasma membrane (PM) proteins or uptake of extracellular materials for transport to the endosome (Murphy et al., 2005). Clathrin-mediated endocytosis (CME) is the major gateway into plant cells (Fan et al., 2015). Although detailed information is available on the roles of endocytosis in animals, researchers have only recently documented that CME is critical for various developmental processes in plants, including cell polarity determination (Van et al., 2011; Wang et al., 2013), male reproductive organ development (Blackbourn and Jackson, 1996; Kim et al., 2013), gametophyte development (Backues et al., 2010), and embryogenesis (Fan et al., 2013; Kitakura et al., 2011). CME is also important in plant responses to abiotic and biotic stresses by internalizing of PM-resident transporters or receptors, such as the boron transporter (BOR1) (Takano et al., 2010), the iron-regulated transporter (IRT1) (Barberon et al., 2011), the auxin efflux transporter PIN-FORMED (PINs) (Dhonukshe et al., 2007), the brassinosteroid receptor BRASSINOSTEROID INSENSITIVE 1 (BRI1) (Di et al., 2013), the bacterial flagellin receptor FLAGELIN SENSING 2 (FLS2) (Robatzek et al., 2006), and the ethylene-inducing xylanase receptor (LeEIX2) (Bar and Avni, 2009).

CME is a complex process that can be divided into at least four steps: the budding of a vesicle, the packaging of cargo into the vesicle, the release of the mature vesicle from the PM, and the fusing of the vesicle with the endosome (Sigismund et al., 2012). Because clathrin cannot directly bind to the PM or to cargoes, the formation of clathrin-coated endocytic vesicles initiates the association of adaptor protein complex 2 (AP2) with the PM, and thus AP2 plays a central role in the initiation of CME. The AP2 complex forms a heterotetrameric complex containing two large subunits (β1-5 and one each of γ/α/δ/ε/ζ), a medium subunit (μ1-5), and a small subunit (σ1-5) (McMahon and Boucrot, 2011). Our understanding of AP2 in plants has been enhanced by the following recent findings: knockdown of the two *Arabidopsis AP2A* genes or overexpression of a dominant-negative version of the medium AP2 subunit, *AP2M*, was shown to significantly impair BRI1 endocytosis

and to enhance brassinosteroid signaling (Di et al., 2013); α and μ adaptins were demonstrated to be crucial for pollen production and viability, as well as elongation of staminal filaments and pollen tubes by modulating the amount and polarity of PINs (Kim et al., 2013); σ adaptin was found to play important roles in the assembly of a functional AP2 complex, and *ap2 σ* loss-of-function *Arabidopsis* exhibited defects in multiple aspects of plant growth and development (Fan et al., 2013).

In addition to the classical AP2 complex, other accessory proteins, including the C-terminal Eps15 homology domain (EHD) proteins, also connect the cargo and membrane lipid to form the CME vesicle. The EHD family contains one member in *Drosophila* and *C. elegans* and four orthologs in mouse and human. All members contain an EHD with two calcium-binding helix-loop-helix motifs (EF-hands), a P-loop with a predicted ATP/GTP binding site, a dynamin-N motif with a nucleotide-binding domain, and a coil-coil region (Bar et al., 2008). The involvement of EHD-containing proteins in CME was described in detail in mammalian cells, in which RME1 was demonstrated to be a key player controlling the recycling of internalized receptors from the endocytic recycling compartment to the PM (Lin et al., 2001). By homologous cloning, two *EHD* genes were isolated from *Arabidopsis* (Bar et al., 2008). The two AtEHD proteins regulated endocytosis in distinct patterns. Over-expression of *AtEHD2* had an inhibitory effect on endocytosis, while down-regulation of *AtEHD1* caused retardation of entry of endocytosed material into plant cells (Bar et al., 2008). However, the mechanisms by which EHD family members linked to CME in plants have not been characterized.

Maize ranks first in total production among major staple cereals and is also an important raw material for biofuel and many other industrial products (Mclaren, 2005). As an important model system for basic biological research, maize has contributed significantly to our knowledge of plant development and evolution, and this understanding has been used to elucidate the developmental mechanisms of maize kernel morphogenesis. The earliest genetic studies performed in maize included analyses of defective kernel (*dek*) mutants. Although several hundred *dek* mutants have been isolated, relatively few corresponding genes have been molecularly cloned

because embryo-lethal alleles are difficult to study (Scanlon and Takacs, 2009).

To better understand maize endosperm filling and maturation, we characterized a maize mutant *ehd1* that is impaired in kernel development and vegetative growth. Positional cloning of *ehd1* and transgenic analysis identified the causative locus as a gene that encodes an EHD-containing protein and that is herein designated as *ZmEHD1*. We show that ZmEHD1 is involved in CME through interaction with the ZmAP2 σ subunit. We further demonstrate that *ZmEHD1* affects the gene expression involved in auxin-related processes and that exogenous 1-NAA application rescues the fertility of the *ehd1* mutant. Our results indicate that, by regulating auxin homeostasis, ZmEHD1-mediated CME is crucial for kernel development and vegetative growth of maize.

Results

The *ehd1* mutant is impaired in kernel development and vegetative growth

The *ehd1* mutant was originally isolated as a shrunken kernel mutant in the screening of natural mutagenesis defective in the filling of maize grains. At 14 days after pollination (DAP), the kernels of *ehd1* homozygous mutant (*ehd1*/*ehd1*) and the wild-type (WT) (*EHD1/EHD1* and *EHD1/ehd1*) resembled each other (Figure 1A). At 16 DAP, the WT kernels were canary-yellow while the *ehd1* mutants were ivory-white (Figure 1A). At maturity, both the endosperm and embryo of *ehd1* mutant were shrunken (Figure 1B), which led to a significant reduction in the 100-kernel weight (Figure 1C). The 100-kernel weight of the WT (26.9 g) was 3-times greater than that of the *ehd1* mutant (Figure 1C).

To analyze the kernel development of the *ehd1* mutant and the WT, we examined immature embryos at 20 DAP by light microscopy. Longitudinal sections indicated that embryo development was slower in the *ehd1* mutant than in the WT (Figure 1D). Endosperm development and texture were also observed by light microscopy. Compared to WT endosperm cells, those of the *ehd1* mutant had less dense cytoplasm and fewer starch granules (Figure 1E).

A paper-culture system was used to measure the germination rates of the WT and

151 the *ehd1* mutant. The germination rate of the *ehd1* mutant was only about 3%, which
152 was far lower than that of the WT (Figure 2A). Relative to the WT seedlings, the
153 germinated *ehd1* seedlings had shorter and fewer primary roots (Figure 2B). Most of
154 the *ehd1* seedlings died before the first two leaves had completely expanded (Figure
155 2C). These results indicated that *ZmEHD1* is essential for maize kernel development
156 and vegetative growth.

157 The mutant was crossed to an inbred line Xun9058. The hybrid F_1 displayed
158 normal kernel as Xun9058. Due to the low germination rate of the *ehd1* mutant, the
159 normal kernels from F_2 ears were planted. Among the 244 F_2 individuals, 79 had the
160 normal kernel phenotype (*EHD1*/*EHD1*), and 165 had the segregation phenotype
161 (*EHD1*/*ehd1*). The segregation ratio followed 1:2 theoretical ratio predicted by a
162 Chi-square test at a 0.05 level (Supplemental Table 1). For each F_2 individual with
163 kernel phenotype segregation, the pattern of shrunken kernel phenotype to normal
164 kernel phenotype fit a 1:3 segregation ratio (Supplemental Table 2). A F_3 population
165 with 376 individuals derived from normal kernels of F_2 selfed ears was also planted to
166 validate the kernel phenotype segregation. Among them, 130 individuals had kernel
167 phenotype (*EHD1*/*EHD1*), and 246 had the segregation phenotype (*EHD1*/*ehd1*)
168 (Supplemental Table 1). These results indicate that this shrunken kernel mutant is
169 controlled by a single recessive gene.
170
171 **Positional cloning of *ZmEHD1***
172 Preliminary genetic mapping of *ZmEHD1* was carried out by BSA using the F_2
173 population, which contained 165 individuals that differed in seed size in the ears. The
174 *ZmEHD1* gene was first mapped to a 2,339-kb region between the simple sequence
175 repeat (SSR) marker umc1650 (17 recombinants) and umc1716 (27 recombinants) on
176 the long arm of chromosome 4 (Figure 3A). Because the germination rate of the *ehd1*
177 mutant was rather low, expanded F_3 mapping population containing ~53,000 normal
178 kernels (*EHD1*/*EHD1* and *EHD1*/*ehd1*) was obtained to increase mapping resolution
179 as described by Zuo et al. (2015). Thirteen new polymorphic SSR markers were
180 developed (Supplemental Table 3), and *ZmEHD1* was eventually mapped to a ~6-kb

region between the SSR markers RM7 (56 recombinants) and RM13 (5 recombinants) (Figure 3A). This region contains two predicted open reading frames (ORFs) (Figure 3A). Sequence analysis revealed three deletions in the 5' UTR and eight single-nucleotide polymorphisms (SNPs) in the ORF of GRMZM2G052740 (Figure 3B). Among the eight SNPs in the ORF of GRMZM2G052740, three led to amino acid replacement between the *ehd1* mutant and the WT (Figure 3B). In addition to GRMZM2G052740, GRMZM2G052720 was also located in this region. Its candidacy as *ZmEHD1* gene was excluded because there was no sequence difference between the WT and the *ehd1* mutant. Thus, we inferred that GRMZM2G052740 was the candidate gene for the *ZmEHD1* locus.

The genomic DNA sequence of GRMZM2G052740 spanned ~4.4-kb and generated a transcript that included 16 exons (Figure 3B). The corresponding 2,209-bp cDNA sequence encoded a polypeptide of 547 amino acids with a molecular mass of ~61 kD (Supplemental Figure 1). BLASTP analysis in GenBank indicated that GRMZM2G052740 is closed related to the *Arabidopsis* EHD-containing proteins, AtEHD1 and AtEHD2 (Supplemental Figure 1). The ZmEHD1 protein shares the typical structure of the EHD family; it has an EH domain with two calcium-binding EF-hands (15-39 aa and 49-84 aa), a P-loop (GQYSTGKT), a dynamin-type guanine nucleotide-binding domain, and a coil-coil domain (Figure 3C).

According to the publicly available maize microarray database (www.qteller.com, Waters et al., 2011), *ZmEHD1* is expressed in various tissues and its mRNA abundance is high in immature cobs (V18), embryos, and endosperms at 12 and 14 DAP. To verify the microarray data, we performed quantitative real-time RT-PCR using RNA isolated from various maize tissues, including roots, leaves, stems, endosperms, and embryos, and the results confirmed the public microarray data (Supplemental Figure 2). We also isolated RNA from the endosperms of the *ehd1* mutant and the WT at 15, 20, 25, and 35 DAP to assess *ZmEHD1* expression levels. The transcripts of *ZmEHD1* were down-regulated during endosperm development in both the *ehd1* mutant and the WT (Figure 3D). Unexpectedly, *ZmEHD1* mRNA abundance at all sampling times in the *ehd1* mutant was higher than in the WT (Figure

3D), indicating that the mutated *ZmEHD1* might be only partly functional.

Validating that *ZmEHD1* is the causative locus by *ZmEHD1* loss-of-function mutants

To determine whether *ZmEHD1* is responsible for the EHD1 locus, we used the CRISPR/Cas9 system to generate *ZmEHD1* loss-of-function mutant (KO). The given gene sequencing in *ZmEHD1* loss-of-function mutants revealed a deletion of 775-bp or 785-bp fragment at the coding sequence, which resulted in a frameshift (Supplemental Figure 3). *ZmEHD1* loss-of-function also led to decreased germination rate as well as retarded vegetative development (Figure 4A and 4B).

An allelism test was performed by crossing KO-1 F_1 (*KO*+/-) and *ehd1* heterozygotes (*ehd1*+/-). The shrunken kernel phenotype (*KO*/*ehd1*) and the WT phenotype (*EHD1*/*EHD1*; *EHD1*/*KO*; *EHD1*/*ehd1*) in the hybrid F_1 ears displayed a 1:3 segregation ratio (Figure 4C, 4D and Supplemental Table 4), indicating that *KO* cannot complement *ehd1*. Meanwhile, the germination rate of the *KO*/*ehd1* mutant was much lower than that of the WT (Figure 4E). These results indicate that *ZmEHD1* is the locus affected by *ehd1*.

The *ehd1* and KO mutant are defective in endocytosis

EHD has usually been identified among proteins involved in endocytosis, vesicle transport, and signal transduction (Lin et al., 2001). To test whether the ZmEHD1 protein is involved in CME in maize, we examined the uptake of N-(3-triethylammonium-propyl)-4-(4-diethylaminophenylhexatrienyl) pyridinium dibromide (FM4-64), a commonly used endocytosis tracer, in the *ehd1* mutant and the WT. Because maize seedlings are relatively large, we could not place the whole plant on the microscope platform as was previously done with 3-day-old *Arabidopsis* plants (Fan et al., 2013). Instead, we detached the similar parts of roots from the *ehd1* mutant and the WT seedlings that had been treated with 5 μM FM4-64 for 10 min to monitor the FM4-64 endocytosis. At 30 minutes after labeling, FM4-64-labelled fluorescent puncta were detected in 28% of the WT root cells (21 of 75 cells), while

241 no FM4-64-labelled fluorescent puncta were detected in *ehd1* root cells (0 of 90 cells)
242 (Figure 5A). Although FM4-64-labelled fluorescent puncta could be detected in root
243 cells of both the WT and the *ehd1* mutant at 60 minutes after labeling,
244 FM4-64-labelled fluorescent puncta were detected in only 19% of the *ehd1* root cells
245 (22 of 117 cells) but in 45% of the WT root cells (45 of 101 cells) (Figure 5A). The
246 effects of ZmEHD1 on endocytosis were further confirmed by the delayed
247 internalization of FM4-64 in *ZmEHD1* knock-out mutants (Figure 5B).

248 To further investigate whether ZmEHD1 was involved in the vesicle traffic
249 pathway, we inhibited endocytic recycling of FM-64 using the fungal toxin brefeldin
250 A (BFA). The accumulation of FM-64 in BFA bodies was clearly observed in the WT
251 when treated with BFA (Figure 5C and 5D). In contrast, the aggregation of FM-64 in
252 BFA bodies remarkably decreased in the *ehd1* mutant and *ZmEHD1* knock-out
253 mutants (Figure 5C and 5D). Compared to the WT, the sizes of FM-64 labeled BFA
254 bodies in the *ehd1* mutant and *ZmEHD1* knock-out mutants decreased by ~67% and
255 ~76%, respectively (Fig. 5C and 5D). These results suggested that ZmEHD1 is
256 important in endocytic transport.

257

258 **Subcellular localization of ZmEHD1 and ZmEHD1$_{mut}$**

259 To determine the subcellular localization of ZmEHD1 protein, yellow fluorescent
260 protein (YFP) fused N-terminally to ZmEHD1 was transiently expressed in tobacco
261 (*N. benthamiana*) leaves under the control of the *CaMV 35S* promoter. In tobacco
262 epidermal cells expressing the YFP-ZmEHD1 fusion protein, the YFP signal was
263 mainly detected in the PM (Supplemental Figure 4A). The localization was confirmed
264 by staining lipid membranes with the red fluorescent probe, FM4-64 (Supplemental
265 Figure 4A). We also cloned the *ZmEHD1* CDS from the *ehd1* mutant and examined
266 the subcellular localization of ZmEHD1$_{mut}$ protein. YFP-ZmEHD1$_{mut}$ signals were
267 aggregated and colocalized with FM4-64 signals in tobacco epidermal cells
268 (Supplemental Figure 4B). This phenomenon was consistently observed in different
269 biological replicates. Thus, we deduced that the mutation in ZmEHD1 affected the
270 subcellular localization of ZmEHD1.

ZmEHD1 interacts with the ZmAP2 σ subunit in yeast and plant

In its drastically reduced fertility and endocytosis, the *ehd1* mutant resembles *Arabidopsis ap2 σ* mutants, in which CME and multiple stages of plant development are impaired (Fan et al., 2013). We hypothesized that ZmEHD1 is involved in CME by virtue of its interaction with the ZmAP2 σ subunit. To test this hypothesis, we cloned the cDNA sequence of the maize AP2 σ subunit (GRMZM2G052713) and introduced it into *Arabidopsis ap2 σ* loss-of-function mutant (Fan et al., 2013). *Arabidopsis ap2 σ* homozygous for the T-DNA insertion was identified by PCR (Supplemental Figure 5A). RT-PCR showed that *ZmAP2 σ* subunit was expressed in the *Arabidopsis ap2 σ* mutant (Supplemental Figure 5B). The transformation of the *Arabidopsisap2 σ* mutant with *ZmAP2 σ* subunit rescued the developmental defects, such as reduced leaf size and fertility (Supplemental Figure 5C). These results suggested that *ZmAP2 σ* subunit has similar functions as *AtAP2 σ* subunit in CME.

The potential interaction between ZmEHD1 and the ZmAP2 σ subunit was first evaluated by a biomolecular fluorescence complementation (BiFC) assay in tobacco leaves and maize mesophyll protoplasts. The ZmEHD1, ZmEHD1$_{mut}$, and ZmAP2 σ subunit constructs were introduced into *N. benthamiana* mesophyll cells or maize mesophyll protoplasts by *A. tumefaciens*-mediated infiltration. The vitality of the *N. benthamiana* mesophyll cells was determined by propidium iodide. Reconstituted YFP signals were observed in the PM when both nYFP-ZmAP2 σ subunit and cYFP-ZmEHD1 constructs were co-expressed (Figure 6A and Supplemental Figure 6). Reconstituted YFP signals were also observed when the nYFP-ZmAP2 σ subunit and cYFP-ZmEHD1$_{mut}$ constructs were co-expressed (Figure 6A and Supplemental Figure 6). Consistent with the subcellular localization of ZmEHD1$_{mut}$, the reconstituted YFP signals were diffused throughout the cells when the nYFP-ZmAP2 σ subunit and cYFP-ZmEHD1$_{mut}$ constructs were co-expressed (Figure 6A and Supplemental Figure 6). This was further verified by the localization of ZmAP2σ subunit in WT maize and *ehd1* mutant (Supplemental Figure 7).

We also used a split-ubiquitin membrane-based yeast two-hybrid system to verify the interaction between the ZmAP2 σ subunit and ZmEHD1 as well as

ZmEHD1$_{mut}$. Both ZmEDH1 and ZmEHD1$_{mut}$ interacted directly with ZmAP2 σ subunit in yeast. The interaction resulted in survival in a medium lacking His and β-galactosidase activity (Figure 6B).

Pull-down experiments using purified His-ZmEHD1/His-ZmEHD1$_{mut}$ to isolate GST-ZmAP2 σ subunit also confirmed the physical interaction between ZmEHD1/ZmEHD1$_{mut}$ and ZmAP2 σ subunit. His-ZmAP2 σ subunit was clearly detected in the pull-down fraction (Figure 6C). These results strongly suggested that ZmEHD1 directly interacts with ZmAP2 σ subunit at the plasma membranes in maize.

Transcriptome profiling of the *ehd1* mutant

To gain insight into the molecular events involved in the *ZmEHD1*-mediated signaling pathway, we compared the whole-transcriptome profiles of endosperms of the *ehd1* mutant and the WT at 15 DAP using RNA-seq. Each sample was represented by two biological replicates, and the libraries were sequenced by Illumina high-throughput sequencing technology. These four RNA libraries yielded more than 0.5 billion raw reads, and approximately 97% of the raw reads remained after adaptor polluted reads, Ns reads, and low quantity reads were trimmed. Of the remaining reads, more than 0.12 billion could be perfectly mapped to maize B73 RefGen_V3.27 (ftp://ftp.ensemblgenomes.org/pub/plants/release-27/fasta/zea_mays). Sequences that could not be mapped to the maize genome were discarded, and only those perfectly mapped were analyzed further. The abundance of each gene was expressed by reads per kilo base million mapped reads (RPKM) (Wagner et al., 2012). We calculated the Pearson's correlation coefficients (*R* value) of the two biological replicates for each treatment to investigate the variability between the replicates. The *R* value of both comparisons exceeded 0.99 (Supplemental Figure 8), indicating a high correlation between biological replicates.

Based on the criteria that the Log_2 fold-change ratio was ≥ 1 and that the adjusted P value was ≤ 0.05, 4,760 genes, including *ZmEHD1*, were identified as differentially expressed genes (DEGs) by DEGseq software (Wang et al., 2010).

Among the DEGs, 2,208 genes were up-regulated and 2,552 genes were down-regulated in the *ehd1* mutant relative to the WT (Supplemental Table 5). The results of RNA-seq were confirmed by quantitative real-time RT-PCR. In agreement with our RNA-seq data, the expression levels of randomly selected GRMZM2G088273, GRMZM2G346897, GRMZM2G067929, and GRMZM2G418119 were lower in the *ehd1* mutant than in the WT (Supplemental Figure 9A). As expected, GRMZM2G156877 and GRMZM2G420988 were expressed at higher levels in the *ehd1* mutant than in WT (Supplemental Figure 9A), demonstrating the reliability of our RNA-seq data. We then performed Gene Ontology (GO; http://bioinfo.cau.edu.cn/agriGO/) analysis to determine the molecular events related to the DEGs. GO analysis indicated that the 4,760 DEGs were highly enriched for biological processed involved in response to stress (GO:0006950, $P = 1.2e^{-12}$), integral to membrane (GO:0016021, $P = 1e^{-5}$), intracellular membrane-bounded organelle (GO:0043231, P = 0.0002), vacuole (GO:0005773, P = 0.0007), starch metabolic processes (GO:0005982, $P = 1.6e^{-5}$), and carbohydrate metabolic processes (GO:0005975, $P = 4.16e^{-5}$).

Interestingly, some of the DEGs have known or presumed functions associated with auxin-mediated signaling pathway (GO:0009734, $P = 1.2e^{-25}$) and response to auxin stimulus (GO:0009733, $P = 2.1e^{-25}$), including AUXIN RESPONSE FACTOR (ARF), AUX/IAA transcription factor, small auxin up-regulated RNA (SAUR), indole-3-acetaldehyde oxidase, auxin transporters, and efflux carrier (Table 1). We randomly chose four of the DEGs listed in Table 1 (GRMZM2G082943, GRMZM2G365188, GRMZM5G809195, and GRMZM2G019799) and validated their difference in expression levels in the *ehd1* mutant vs. the WT by quantitative real-time RT-PCR (Supplemental Figure 9B). These results indicated that *ZmEHD1* might affect auxin homeostasis in maize.

Auxin distribution and ZmPIN1a-YFP localization in the *ehd1* mutant

To test the hypothesis that *ZmEHD1* might affect auxin homeostasis in maize, we first explored the gravitropic response by examining mesocotyl-coleoptiles. We placed the

upright mesocotyl-coleoptiles in the horizontal direction. In contrast to less than 4 h for the recovered vertical growth of WT, it took about 5 h for the *ehd1* mutant and *ZmEHD1* knock-out mutants to recover vertical growth under the same condition (Figure 7A). The free IAA content in kernels of the *ehd1* mutant and the WT at 15 DAP were determined. The free IAA content in the kernels of the *ehd1* mutant was 2,558 pg mg^{-1} FW, which was ~30% lower than that in the WT (Figure 7B).

To further demonstrate that ZmEHD1 regulates auxin homeostasis in maize, we first crossed the auxin-responsive ZmDR5::RFP reporter maize with *ehd1* mutant to examine the auxin distribution in the root tips of *ehd1* mutant. The RFP signals were significantly reduced in the root caps in *ehd1* mutant (Figure 7C). We also crossed the ZmPIN1a::YFP line with *ehd1* mutant. The YFP signals in the roots of *ehd1* mutant showed more diffuse localization than that in *PIN1a::YFP EHD1* line, and could be detected in root cortex (Figure 7D). These results suggested that auxin homeostasis was altered in *ehd1* mutant.

1-NAA application rescues the fertility of the *ehd1* mutant

To further verify that the rather low fertility of the *ehd1* mutant and *ZmEHD1* knock-out mutant was caused by auxin homeostasis, we attempted to rescue the phenotypic defects of *ehd1* mutant and *ZmEHD1* knock-out mutants by exogenous application of the active auxin compound, 1-naphthaleneacetic acid (1-NAA). The seeds of the *ehd1* mutant and *ZmEHD1* knock-out mutants were rinsed in water or in four increasing concentrations of 1-NAA for 12 h, and then germinated in the paper-culture system. Little or no phenotypic rescue of the *ehd1* mutant was observed when 30 mg L^{-1} 1-NAA or water alone was applied (Figure 8A). However, the germination rate of *ehd1* mutant and *ZmEHD1* knock-out mutant was significantly increased when treated with low concentrations of 1-NAA (Figure 8A). Also, when treated with low concentrations of 1-NAA, the *ehd1* mutant and *ZmEHD1* knock-out mutant survived after its first two leaves had completely expanded (Figure 8B). In contrast to IAA, exogenous GA3 had no effect on the germination of the *ehd1* mutant and *ZmEHD1* knock-out mutant (Supplemental Figure 10). Overall, these results

391 demonstrated that the phenotypic defects of the *ehd1* mutant could be rescued by
392 exogenous application of 1-NAA.
393
394 **Discussion**
395 In the present research, we characterized the *ehd1* mutant, which is impaired in kernel
396 development and vegetative growth, and used positional cloning and transgenic
397 validation to verify that the *ehd1* gene encodes an EHD protein. The results of an
398 FM4-64 uptake experiment, split-ubiquitin membrane-based yeast two-hybrid system,
399 BiFC and pull-down assay indicated that ZmEHD1 is involved in CME through its
400 interaction with the ZmAP2 σ subunit. Additionally, the transcriptome profiling of the
401 ehd1 mutant, the auxin distribution and ZmPIN1a-YFP localization in the *ehd1*
402 mutant, and the rescue of the mutant phenotypes following the exogenous application
403 of 1-NAA revealed that the ZmEHD1-mediated endocytosis mainly affects auxin
404 homeostasis in maize.
405 In *Arabidopsis*, AP2 σ subunit is primarily recruited from the cytoplasm to the
406 PM to initiate clathrin-coated endocytic vesicle formation (Fan et al., 2013; Fan et al.,
407 2015). The developmental defects of *ap2 σ* loss-of-function *Arabidopsis*, such as
408 reduced leaf size and fertility, could be rescued by *ZmAP2 σ* cDNA, suggesting that
409 *ZmAP2 σ* subunit has similar functions as *AtAP2 σ* subunit in CME. Microarray data
410 revealed that the AP2 σ subunit is ubiquitously expressed in various tissues
411 throughout maize development (Sekhon et al., 2011), which is consistent with the
412 expression pattern of *ZmEHD1*. Based on the direct interaction between the ZmAP2σ
413 subunit and ZmEHD1 at the PM as demonstrated by BIFC, pull-down assay and
414 split-ubiquitin membrane-based yeast two-hybrid system in the current study, we
415 suspected that ZmEHD1 contributes to CME by interacting with the ZmAP2 σ
416 subunit.
417 The naturally occurring *ehd1* mutant had amino acid substitutions in three
418 positions. Of these, the V/A substitution was in a linker region. The other two
419 mutations were in the coil-coil domain of ZmEHD1. The coil-coil domain was
420 responsible for protein-protein interactions (Bar et al., 2009; Sharma et al., 2008).

421 Here, we showed that the subcellular location of ZmEHD1$_{mut}$ was obviously different
422 from that of ZmEHD1. Though ZmEHD1$_{mut}$ could directly interact with ZmAP2σ
423 subunit, the PM was not the main location for interaction between ZmEHD1$_{mut}$ and
424 the ZmAP2σ subunit. The impaired clathrin-coated endocytic vesicle formation
425 and/or the recycling of the ZmAP2 σ subunit from the endosome to the PM should be
426 the major contributor to phenotypes observed in the *ehd1* mutant.

427 *Arabidopsis ARF2* controls seed size by repressing cell proliferation (Schruff et
428 al., 2006); in rice, activation of *BIG GRAIN1* (BG1) significantly improves grain size
429 by regulating auxin transport (Liu et al., 2015); *TGW6*, an IAA-glucose hydrolase,
430 negatively regulates endosperm development of rice (Ishimaru et al., 2013). Analyses
431 of a seed-specific viable maize mutant, defective endosperm 18 (*de18*), demonstrated
432 that the *ZmYUC1* gene (which is critical for IAA biosynthesis) is essential for normal
433 endosperm development in maize (Bernardi et al., 2012). Thus, auxin biosynthesis,
434 transport and signaling might coordinate to regulate vegetative and reproductive
435 development in maize (Gallavotti et al., 2008; Li and Li, 2016). The current results
436 with maize show that *ARFs*, indole-3-acetaldehyde oxidase, auxin transporters, and
437 efflux carrier are differentially expressed in the *ehd1* mutant vs. the WT; that the
438 concentration of free IAA is lower in the *ehd1* mutant than in the WT; that the auxin
439 distribution and ZmPIN1a-YFP localization were altered in the *ehd1* mutant; and that
440 exogenous application of 1-NAA rescues the phenotypes of the *ehd1* mutant. These
441 results suggest that the growth defects of the *ehd1* mutant result from the loss of auxin
442 homeostasis.
443

444 **Materials and methods**

445 **Plant materials**

446 The ZmPIN1a::YFP and ZmDR5::mRFP lines were kindly provided by Lixing Yuan
447 (China Agricultural University). The maize mutant ehd1 was isolated by screening for
448 natural mutants defective in grain filling. To construct mapping population, the mutant
449 was crossed with inbred line Xun9058 in the winter of 2011 in Sanya, Hainan
450 Province. Xun9058 is the male parent of the elite hybrid Xundan20 and has been

widely used in the breeding of hybrid maize in China. F_2 individuals were obtained by selfing the F_1 plants in the summer of 2012 in Zhengzhou, Henan Province. The site (113°42′E, 34°48′N) is located in central China and has an average annual temperature of 14.3 °C and an average annual rainfall of 640.9 mm. A F_2 population with 165 individuals was used to map the preliminary location of *ZmEHD1* gene. Normal kernels from F_3 segregation ears were used for fine mapping of the candidate gene. The F_3 population contains ~53,000 individuals. A small piece of each F_3 kernel was chipped and genotyped before planting. At harvest stage, the ear phenotype was investigated to verify the kernel segregation of each individual. Two markers, bnlg589 and RM1, were closely linked to the locus to determine recombined individuals.

From F_2 generation, the normal kernels from segregation ears were analyzed by closely linked marker with *ZmEHD1* gene and the recombined individuals were selfed. This process was continued for five generations to construct nearly isogenic lines (NILs). The NILs were used as WT.

Molecular markers

Bulked segregant analysis (BSA) was used to detect the genetic linkage of the *ZmEHD1* gene (Michelmore et al., 1991) and 1082 SSR markers from the maize genome database (www.maizegdb.org) were tested for polymorphism in the two parents and the two bulks. To develop new markers for fine mapping, the sequence of the B73 reference genome between markers bnlg589 and umc2289 on chromosome 4 was downloaded from MaizeGDB (http://www.maizegdb.org/). SSR-Hunter software was used find simple sequence repeats (SSRs). After BLAST was performed (http://blast.ncbi.nlm.nih.gov/Blast.cgi), SSRs with single copy were developed to new markers with PRIMER 5.0. The newly designed SSRs were tested by polyacrylamide gel electrophoresis (PAGE) for polymorphism in the *ehd1* mutant, Xun9058, pooled samples of normal kernels (*EHD1/EHD1* and *EHD1/ehd1*) or shrunken kernels (*ehd1/ehd1*). SSRs with polymorphism were used for subsequent fine mapping. The sequences of the primers used for mapping are listed in Supplemental Table 3.

481 **Transgenic functional validation**

482 The CRISPR/Cas9-mediated *ZmEHD1* editing was performed as described by Xing et
483 al. (2014) with some modifications. In brief, two gRNAs that direct target sequences
484 located at nucleotides 16 and 791 of *ZmEHD1* were produced using primers listed in
485 Supplemental Table 3. Thereafter, the fragments were cloned into the pBUE411
486 vector using the *Bsa*I restriction site by T4 Ligase reaction. The plasmid contained the
487 *Streptomyces* hygroscopicus phosphinothricin acetyltransferase gene (*bar*) under the
488 control of a *CaMV 35S* promoter and was electroporated into *A. tumefaciens* EHA105.
489 Immature embryos of maize inbred line ZZC01 were transformed by co-cultivation
490 with EHA105 at Life Science and Technology Center of China National Seed Group
491 Co., LTD. Transformants were selected with gradually increasing concentrations of
492 Bialaphos. T_2 homozygous lines were sequenced to ensure that *ZmEHD1* was
493 knocked out.

494 For *Arabidopsis* transformation, the cDNAs of *ZmAP2 σ* subunit without 3' UTR
495 were amplified by PCR. The corresponding products were introduced into the
496 pENTR^{TM}/D-TOPO vector (Invitrogen) and cloned into pMDC32 by LR reactions
497 (Invitrogen). The plasmid was electroporated into *A. tumefaciens* GV3101 and was
498 transformed into *Arabidopsis* by the floral dip method (Clough and Bent, 1998).
499 Transgenic plants were selected with the use of 35 μg ml^{-1} hygromycin. The
500 sequences of the primer pairs used in the experiments are listed in Supplemental
501 Table 3.

502

503 **Expression analysis of *ZmEHD1***

504 Total RNA was extracted from the WT and the *ehd1* mutant with the RNeasy plant
505 mini kit. The RNA was used for the synthesis of first-strand cDNA with SuperScript
506 III first-strand synthesis supermix (Invitrogen). Quantitative real-time RT-PCR was
507 carried out in an ABI 7500 system using the SYBR Premix Ex TaqTM (perfect real
508 time) kit (TaKaRaBiomedicals), with 18S rRNA and *Actin* as controls. Primers
509 designed to detect the transcription level of *ZmEHD1* were listed in Supplemental
510 Table 3. The relative expression level was calculated using the comparative Ct

511 method. Each experiment was replicated at least three times.

512

513 **Subcellular localization of ZmEHD1**

514 The full-length *ZmEHD1* and *ZmEHD1*$_{mut}$ coding region was amplified from the WT
515 and the *ehd1* mutant. To generate the *ZmEHD1* expression plasmids, the 1644-bp
516 fragments were cloned into the pCPB vector, which was fused to an YFP protein in
517 the N terminus using the *Bam*HI restriction site by In-Fusion reaction. The plasmid
518 was electroporated into *A. tumefaciens* GV3101 and was transiently expressed in
519 tobacco epidermal cells as described previously (Li et al., 2008). To stain the PM of
520 epidermal cells, 5 μM FM4-64 was infiltrated into tobacco leaves for 3 h before
521 observation. YFP/FM-64 images were collected with a Zeiss LSM700 confocal
522 microscope.

523

524 **Split-ubiquitin yeast two-hybrid assay**

525 The split-ubiquitin two-hybrid system was used to detect the interactions between
526 membrane proteins. The assay was carried out according to the instructions provided
527 with the DUALmembrane Kit (Dualsystems Biotech). The full-length coding regions
528 of the *ZmAP2* σ subunit, *ZmEHD1* and *ZmEHD1*$_{mut}$ were amplified and cloned into
529 the vectors pST3-STE and pPR3-N NubG using the *Sfi*I restriction site by In-Fusion
530 reaction. Vectors were co-transformed into yeast strain NMY51. The interactions were
531 assessed by the growth of yeast colonies on synthetic minimal medium containing 7.5
532 mM 3-aminnotriazole without Leu, Trp, His and Ade and also by chloroform overlay
533 β-galactosidase plate assay (Duttweiler, 1996).

534

535 **Bimolecular fluorescence complementation (BiFC) assays**

536 The coding sequences of the *ZmAP2* σ subunit, *ZmEHD1* and *ZmEHD1*$_{mut}$ were
537 amplified using specific primers listed in Table S1, and were cloned into the
538 pSPYNE-35S or pSPYCE-35S binary vectors using the *Bam*HI restriction site. The
539 various combinations of *ZmAP2* σ subunit, *ZmEHD1*, and *ZmEHD1*$_{mut}$ expression
540 vectors were transiently expressed in 3-week-old *N. benthamiana* leaves by

Agrobacterium-mediated infiltration (strain EHA105). YFP images were obtained 3 days after infiltration with a Zeiss LSM700 confocal microscope.

Pull-down analysis

The full-length coding sequences of *ZmEHD1, ZmEHD1*$_{mut}$ and *ZmAP2* σ subunit were individually subcloned into the pET-28a(+) and pGEX-4T-1 vectors using the *Bam*HI restriction site by In-Fusion reaction. The resulting constructs were verified by sequencing. His-ZmEHD1, His-ZmEHD1$_{mut}$, GST and GST-ZmAP2 σ subunit were expressed in *Escherichia coli* BL21.

For the *in vivo* pull-down analysis, 10 μg of purified His-ZmEHD1, His-ZmEHD1$_{mut}$ were incubated with GST-ZmAP2 σ subunit or GST bound to glutathione-Sepharose™ 4B (GE Healthcare) for 4 h at 4 °C on a rotary shaker. Precipitated beads were washed six times with washing buffer. Washed beads were boiled with 50 μL of 1 × SDS sample buffer for 5 min and subjected to SDS-PAGE and immunoblot analysis.

FM4-64 internalization assay

FM4-64 internalization assays were carried out to evaluate the rate of endocytosis as described by Fan et al. (2013) with some modifications. WT and *ehd1* seedlings were incubated in half-strength Hoagland's nutrient solution containing 5 μM FM4-64 for 10 min at room temperature. The roots were then cut and transferred to glass slides. The FM4-64 internalization was monitored at indicated durations at room temperature with a Zeiss LSM700 confocal microscope.

RNA-seq analysis

At 15 DAP, total RNA was extracted from the endosperms of the *ehd1* mutant and the WT with TRIZOL reagent (Invitrogen), and 3 μg of total RNA was used as input material for construction of the RNA libraries. The RNA-sequencing libraries were constructed with NEBNext® Ultra™ RNA Library Prep Kit for Illumina® (NEB, USA). In brief, mRNA was purified from total RNA using poly-T oligo-attached

571 magnetic beads. The enriched mRNA was then fragmented. The random hexamers
572 were used for first-strand cDNA synthesis. After second-strand cDNA synthesis,
573 terminal repair, and poly(A) tail and sequencing oligonucleotide adaptors ligation, the
574 fragments were purified and subsequently amplified by PCR. The insert size was
575 assessed with the Agilent Bioanalyzer 2100 system (Agilent Technologies, CA).
576 Finally, the libraries of inserting cDNAs with 200-bp in size were generated and
577 sequenced with the IlluminaHiseq 2500 platform (ANROAD, Beijing, China).

578 The raw reads were produced after exclusion of low quality reads and 5' and 3'
579 adaptor contaminants. The unique RNAs were aligned to the maize RefGen_V3.27
580 (ftp://ftp.ensemblgenomes.org/pub/plants/release-27/fasta/zea_mays). Only perfectly
581 matching sequences were considered for further analysis. The count information was
582 used to determine normalized gene expression levels as RPKM (Wagner et al., 2012).
583 Multiple testing with the Benjamini-Hochberg procedure for false discovery rate
584 (FDR) was taken into account by using an adjusted P-value. Genes were considered to
585 be differentially expressed if the Log_2 fold-change ratio was ≥ 1 and if the adjusted P
586 value was < 0.05 according to the DEGseq method (Wang et al., 2010).
587

588 **Free IAA analysis**

589 At 15 DAP, kernels of the WT and the *ehd1* mutant were collected and frozen in
590 liquid nitrogen. A 200-mg (fresh weight) sample of WT and *ehd1* kernels was finely
591 ground in liquid nitrogen and then extracted with 1 ml of methanol containing
592 antioxidant and $^{2}H_2$-IAA (internal standard, CDN Isotopes) at 4°C for 24 h. After
593 centrifugation, the extract was purified with an Oasis Max solid phase extract
594 cartridge (150 mg/6 cc; Waters). IAA was quantified using UPLC-MS/MS consisting
595 of a UPLC system (ACQUITY UPLC, Waters) and a triple quadruple tandem mass
596 spectrometer (Quattro Premier XE, Waters) as described by Wang et al. (Wang et al.,
597 2015). Four independent biological replicates and two technical repeats were
598 performed for the WT and the *ehd1* mutant.
599

600 **Phytohormone treatments**

For phytohormone treatments, WT and *ehd1* mutant seeds were immersed in water and the indicated concentrations of 1-NAA for 12 h or GA3 for 24 h. The seeds were then kept at 22 °C in the dark for 120 h for germination. A seed was scored as germinated if its radicle protruded through the seed coat.

Additional information

Funding

Funder	Grant reference number	Author
National Key Research and Development Program of China	2016YFD0101002	Wen-Xue Li
National Basic Research Program of China Grant	31370303	Jihua Tang

The funders had no role in study design, data collection and interpretation, or the decision to submit the work for publication.

Author contributions

J.T. and W.X.L. designed the research; Y.W., W.L., H.W., Q.D. and Z.F. performed the research; W.X.L. and J.T. analyzed the data and wrote the article.

References

Backues SK, Korasick DA, Heese A, Bednarek SY. 2010. The *Arabidopsis* dynamin-related protein2 family is essential for gametophyte development. *Plant Cell* **22**:3218-3231. DOI: https://doi.org/10.1105/tpc.110.077727, PMID: 20959563

Bar M, Aharon M, Benjamin S, Rotblat B, Horowitz M, Avni A. 2008. AtEHDs, novel *Arabidospsis* EH-domain-containing proteins involved in endocytosis. *Plant J.* **55**:1025-1038. DOI: https://doi.org/10.1111/j.1365-313X.2008.03571.x, PMID: 18547399

Bar M, Avni A. 2009. EHD2 inhibits ligand-induced endocytosis and signaling of the

623 leucine-rich repeat receptor-like protein LeEix2. *Plant J*. **59**:600-611. DOI :
624 https://doi.org/10.1111/j.1365-313X.2009.03897.x, PMID: 19392695
625 Bar M, Sharfman M, Schuster S, Avni A. 2009. The coiled-coil domain of EHD2
626 mediates inhibition of LeEix2 endocytosis and signaling. *PLoS ONE* **4**:e7973.
627 DOI: https://doi.org/10.1371/journal.pone.0007973, PMID:19936242
628 Barberon M, Zelazny E, Robert S, Conéjéro G, Curie C, Friml J, Vert G. 2011.
629 Monoubiquitin-dependent endocytosis of the iron-regulated transporter 1 (IRT1)
630 transporter controls iron uptake in plants. *PNAS* **108**:E450-E458. DOI:
631 https://doi.org/10.1073/pnas.1100659108, PMID: 21628566
632 Bernardi J, Lanubile A, Li QB, Kumar D, Kladnik A, Cook SD, Ross JJ, Marocco A,
633 Chourey PS. 2012. Impaired auxin biosynthesis in the defective endosperm18
634 mutant is due to mutational loss of expression in the *ZmYuc1* gene encoding
635 endosperm-specific YUCCA1 protein in maize. *Plant Physiol.* **160**:1318-1328.
636 DOI: https://doi.org/10.1104/pp.112.204743, PMID: 22961134
637 Blackbourn HD, Jackson AP. 1996. Plant clathrin heavy chain: sequence analysis and
638 restricted localization in growing pollen tubes. *Journal of Cell Science*
639 **109**:777-786. PMID: 8718669
640 Clough SJ, Bent AF. 1998. Floral dip: a simplified method for
641 Agrobacterium-mediated transformation of *Arabidopsis thaliana*. *Plant J.*
642 **16**:735-743. DOI: https://doi.org/10.1046/j.1365-313x.1998.00343.x, PMID:
643 10069079
644 Dhonukshe P, Aniento F, Hwang I, Robinson DG, Mravec J, Stierhof YD, Friml J.
645 2007. Clathrin-mediated constitutive endocytosis of PIN auxin efflux carriers in
646 *Arabidopsis*. *Current Biology* **17**:520-527. DOI:
647 https://doi.org/10.1016/j.cub.2007.01.052, PMID: 17306539
648 Di Rubbo S, Irani NG, Kim SY, Xu ZY, Gadeyne A, Dejonghe W, Vanhoutte I,
649 Persiau G, Eeckhout D, Simon S, Song K, Kleine-Vehn J, Friml J, De Jaeger G,
650 Van Damme D, Hwang I, Russinova E. 2013. The clathrin adaptor complex AP-2
651 mediates endocytosis of BRASSINOSTEROID INSENSITIVE1 in *Arabidopsis*.
652 *Plant Cell* **25**:2986-2997. DOI: https://doi.org/10.1105/tpc.113.114058, PMID:

23975899

Duttweiler HM. 1996. A highly sensitive and non-lethal beta-galactosidaseplate assay for yeast. *Trends in Genetics* **12**:340-341. DOI: https://doi.org/10.1016/S0168-9525(96)80008-4, PMID: 8855661

Fan L, Hao H, Xue Y, Zhang L, Song K, Ding Z, Botella MA, Wang H, Lin J. 2013. Dynamic analysis of *Arabidopsis* AP2 σ subunit reveals a key role in clathrin-mediated endocytosis and plant development. *Development* **140**:3826-3837. DOI: https://doi.org/10.1242/dev.095711, PMID: 23924631

Fan L, Li R, Pan J, Ding Z, Lin J. 2015. Endocytosis and its regulation in plants. *Trends in Plant Science* **20**:388-397. DOI: https://doi.org/10.1016/j.tplants.2015.03.014, PMID: 25914086

Gallavotti A, Barazesh S, Malcomber S, Hall D, Jackson D, Schmidt RJ, McSteen P. 2008. Sparse inflorescence1 encodes a monocot-specific YUCCA-like gene required for vegetative and reproductive development in maize. *PNAS* **105**:15196-15201. DOI: https://doi.org/10.1073/pnas.0805596105, PMID: 18799737

Ishimaru K, Hirotsu N, Madoka Y, Murakami N, Hara N, Onodera H, Kashiwagi T, Ujiie K, Shimizu B, Onishi A, Miyagawa H, Katoh E. 2013. Loss of function of the IAA-glucose hydrolase gene TGW6 enhances rice grain weight and increases yield. *Nature Genetics* **45**:707-711. DOI: https://doi.org/10.1038/ng.2612, PMID: 23583977

Kim SY, Xu ZY, Song K, Kim DH, Kang H, Reichardt I, Sohn EJ, Friml J, Juergens G, Hwang I. 2013. Adaptor protein complex 2-mediated endocytosis is crucial for male reproductive organ development in *Arabidopsis*. *Plant Cell* **25**:2970-2985. DOI: https://doi.org/10.1105/tpc.113.114264, PMID: 23975898

Kitakura S, Vanneste S, Robert S, Löfke C, Teichmann T, Tanaka H, Frimla J. 2011. Clathrin mediates endocytosis and polar distribution of PIN auxin transporters in *Arabidopsis*. *Plant Cell* **23**: 1920-1931. DOI: https://doi.org/10.1105/tpc.111.083030, PMID: 21551390

Li N, Li Y. 2016. Signaling pathways of seed size control in plants. *Current Opinion*

683 *in Plant Biology* **33**:23-32. DOI: https://doi.org/10.1016/j.pbi.2016.05.008,
684 PMID: 27294659

685 Li WX, Oono Y, Zhu J, He XJ, Wu JM, Iida K, Lu XY, Cui X, Jin H, Zhu JK. 2008.
686 The *Arabidopsis NFYA5* transcription factor is regulated transcriptionally and
687 posttranscriptionally to promote drought resistance. *Plant Cell* **20**:2238-2251.
688 DOI: https://doi.org/10.1105/tpc.108.059444, PMID: 18682547

689 Lin SX, Grant B, Hirsh D, Maxfield FR. 2001. Rme-1 regulates the distribution and
690 function of the endocytic recycling compartment in mammalian cells. *Nature*
691 *Cell Biology* **3**: 567-572. DOI: https://doi.org/10.1038/35078543, PMID:
692 11389441

693 Liu L, Tong H, Xiao Y, Che R, Xu F, Hu B, Liang C, Chu J, Li J, Chu C. 2015.
694 Activation of Big Grain1 significantly improves grain size by regulating auxin
695 transport in rice. *PNAS* **112**: 11102-11107. DOI:
696 https://doi.org/10.1073/pnas.1512748112, PMID: 26283354

697 Mclaren JS. 2005. Crop biotechnology provides an opportunity to develop a
698 sustainable future. *Trends in Biotechnology* **23**: 339-342. DOI:
699 https://doi.org/10.1016/j.tibtech.2005.04.004, PMID: 15978317

700 McMahon HT, Boucrot E. 2011. Molecular mechanism and physiological functions of
701 clathrin-mediated endocytosis. *Nature Reviews Molecular Cell Biology* **12**:
702 517-533. DOI: https://doi.org/10.1038/nrm3151, PMID: 21779028

703 Michelmore RW, Paran I, Kesseli V. 1991. Identification of markers linked to disease
704 resistance genes by bulked segregant analysis: a rapid method to detect markers
705 in specific genomic region is by using segregating population. *PNAS* **88**:
706 9828-9832. DOI: https://doi.org/10.1073/pnas.88.21.9828, PMID: 1682921

707 Murphy AS, Bandyopadhyay A, Holstein SE, Peer WA. 2005. Endocytic cycling of
708 PM proteins. *Annual Review of Plant Biology* **56**: 221-251. DOI:
709 https://doi.org/10.1146/annurev.arplant.56.032604.144150, PMID: 15862095

710 Robatze S, Chinchilla D, Boller T. 2006. Ligand-induced endocytosis of the pattern
711 recognition receptor FLS2 in *Arabidopsis*. *Genes & Development* **20**: 537-542.
712 DOI: https://doi.org/10.1101/gad.366506, PMID: 16510871

713 Scanlon MJ, Takacs EM. 2009. Kernel biology. In J Bennetzen, S Hake, eds,
714 Handbook of Maize, Its Biology. Springer, New York, pp 121-129.
715 Schruff MC, Spielman M, Tiwari S, Adams S, Fenby N, Scott RJ. 2006. The AUXIN
716 RESPONSE FACTOR 2 gene of Arabidopsis links auxin signalling, cell division,
717 and the size of seeds and other organs. *Development* **133**: 251-261. DOI:
718 https://doi.org/10.1242/dev.02194, PMID: 16339187
719 Sekhon RS, Lin H, Childs KL, Hansey CN, Buell CR, de Leon N, Kaeppler SM. 2011.
720 Genome-wide atlas of transcription during maize development. *Plant J* **66**:
721 553-563. DOI: https://doi.org/10.1111/j.1365-313X.2011.04527.x, PMID:
722 21299659
723 Sharma M, Naslavsky N, Caplan S. 2008. A role for EHD4 in the regulation of early
724 endosomal transport. *Traffic* **9**: 995-1018. DOI:
725 https://doi.org/10.1111/j.1600-0854.2008.00732.x, PMID: 18331452
726 Sigismund S, Confalonieri S, Ciliberto A, Polo S, Scita G, Di Fiore PP. 2012.
727 Endocytosis and signaling: cell logistics shape the eukaryotic cell plan.
728 *Physiological Reviews* **92**: 273-366. DOI:
729 https://doi.org/10.1152/physrev.00005.2011, PMID: 22298658
730 Takano J, Tanaka M, Toyoda A, Miwa K, Kasai K, Fuji K, Onouchi H, Naito S,
731 Fujiwarab T. 2010. Polar localization and degradation of *Arabidopsi*s boron
732 transporters through distinct trafficking pathways. *PNAS* **107**: 5220-5225. DOI:
733 https://doi.org/10.1073/pnas.0910744107, PMID: 20194745
734 Van Damme D, Gadeyne A, Vanstraelen M, Inze D, VanMontagu MC, De Jaeger G,
735 Russinova E, Geelen D. 2011. Adaptin-like protein TPLATE and clathrin
736 recruitment during plant somatic cytokinesis occurs via two distinct pathways.
737 *PNAS* **108**: 615-620. DOI: https://doi.org/10.1073/pnas.1017890108, PMID:
738 21187379
739 Wagner GP, Kin K, Lynch VJ. 2012. Measurement of mRNA abundance using
740 RNA-Seq data: RPKM measure is inconsistent among samples. *Theory Biosci*
741 **131**: 281-285. DOI: https://doi.org/10.1007/s12064-012-0162-3 PMID:
742 22872506

743 Wang B, Chu J, Yu T, Xu Q, Sun X, Yuan J, Xiong G, Wang G, Wang Y, Li J. 2015.
744 Tryptophan-independent auxin biosynthesis contributes to early embryogenesis
745 in Arabidopsis. *PNAS* **112**: 4821-4826. DOI:
746 https://doi.org/10.1073/pnas.1503998112, PMID: 25831515
747 Wang C, Yan X, Chen Q, Jiang N, Fu W, Ma B, Liu J, Li C, Bednarek SY, Pan J. 2013.
748 Clathrin light chains regulate clathrin-mediated trafficking, auxin signaling, and
749 development in *Arabidopsis*. *Plant Cell* **25**: 499-516. DOI:
750 https://doi.org/10.1105/tpc.112.108373, PMID: 23424247
751 Wang L, Feng Z, Wang X, Wang X, Zhang X. 2010. DEGseq: an R package for
752 identifying differentially expressed genes from RNA-seq data. *Bioinformatics* **26**:
753 136-138. DOI: https://doi.org/10.1093/bioinformatics/btp612, PMID:19855105
754 Waters AJ, Makarevitch I, Eichten SR, Swanson-Wagner RA, Yeh CT, Xu W,
755 Schnable PS, Vaughn MW, Gehring M, Springer NM. 2011. Parent-of-origin
756 effects on gene expression and DNA methylation in the maize endosperm. *Plant*
757 *Cell* **23**: 4221-4233. DOI: https://doi.org/10.1105/tpc.111.092668, PMID:
758 22198147
759 Xing HL, Dong L, Wang ZP, Zhang HY, Han CY, Liu B, Wang XC, Chen QJ. 2014. A
760 CRISPR/Cas9 toolkit for multiplex genome editing in plants. *BMC Plant Biology*
761 **14**: 327. DOI: https://doi.org/10.1186/s12870-014-0327-y, PMID: 25432517
762 Zuo W, Chao Q, Zhang N, Ye J, Tan G, Li B, Xing Y, Zhang B, Liu H, Fengler KA,
763 Zhao J, Zhao X, Chen Y, Lai J, Yan J, Xu M. 2015. A maize wall-associated
764 kinase confers quantitative resistance to head smut. *Nature Genetics* **47**: 151-157.
765 DOI: https://doi.org/10.1038/ng.3170, PMID: 25531751
766
767
768
769
770
771
772

773 **Table 1** Differentially expressed genes involved in auxin-related processes in the *ehd1*
774 mutant.

Gene ID	Annotation[1]	Log_2 Fold-change (*ehd1*vs.WT)	Adjusted P value
GRMZM2G126260	PIN10a	-5.53	0.0007
GRMZM2G149481	Auxin transporter-like protein 3	3.40	0.0023
GRMZM2G127949	Auxin transporter-like protein 1	1.94	$2.10e^{-16}$
GRMZM2G019799	Indole-3-acetaldehyde oxidase-like	1.39	0.0006
GRMZM2G082943	ZAR9	-2.46	$2.04e^{-12}$
GRMZM2G065244	Auxin-induced in root cultures protein 12-like	1.01	0.0158
GRMZM2G079957	AUX17	-1.17	0.0061
GRMZM2G130953	AUX22	1.80	0.0004
GRMZM2G081158	Auxin response factor 25-like	1.36	$2.61e^{-6}$
GRMZM2G475263	Auxin response factor 1	1.15	$7.27e^{-11}$
GRMZM2G028980	Auxin response factor 6 isoform X1	1.53	$1.62e^{-12}$
GRMZM5G808366	Auxin response factor 5	1.99	0.0038
GRMZM2G137413	Auxin response factor 14	2.06	$5.04e^{-41}$
GRMZM2G064371	Auxin binding protein-like protein	1.38	0.0001
GRMZM2G365188	SAUR23	-3.37	0.0004
GRMZM2G414727	SAUR56	-2.95	$1.12e^{-26}$
GRMZM2G059138	SAUR33	-2.01	$7.63e^{-8}$
GRMZM2G121309	IAA7	1.16	$5.26e^{-8}$
GRMZM2G030465	IAA9	3.19	0.0146
GRMZM2G077356	IAA13	2.90	$9.83e^{-18}$
GRMZM5G809195	IAA14	-2.12	0.0046
GRMZM2G115357	IAA24	-1.25	$8.09e^{-7}$
GRMZM2G048131	IAA26	inf	0.0002

775 [1]Annotation is based on maize IDs

776 **Figure Legends**

777 **Figure 1. Phenotypes of the maize *ehd1* mutant kernels.** (A) F_2 ears of *ehd1* ×
778 Xun9058 at 14 or 16 days after pollination (DAP). The red arrows indicated the *ehd1*
779 kernels. Scale bars = 1 cm. (B) The mature kernels of wild type (WT) and *ehd1*
780 mutant randomly selected from F_2 ears of *ehd1* × Xun9058. Scale bars = 0.5 cm. (C)
781 100-grain weight of the WT and the *ehd1* mutant. Values are means and standard
782 errors (n=4). ** indicates a significant difference ($P < 0.01$) between the WT and the
783 *ehd1* mutant. (D) Comparison of WT and *ehd1* embryos at 20 DAP. The sections
784 stained with Safranin and Fast Green. Scale bars = 5 mm. (E) Microstructure of WT
785 and *ehd1* endosperms at 15 DAP. The sections stained with fuchsin. Scale bars = 5
786 mm.

787

788 **Figure 2. *ZmEHD1* is required for normal growth and development of maize.** (A)
789 Germination of the WT and the *ehd1* mutant. Values are means and standard errors of
790 approximately 100 seeds from three independent experiments. (B) Root number and
791 root elongation of the WT and the *ehd1* mutant. Values are means and standard errors
792 (n=5). ** indicates a significant difference ($P < 0.01$) between the WT and the *ehd1*
793 mutant. (C) Phenotypes of WT and *ehd1* seedlings (n=30). Representative photograph
794 is shown.

795

796 **Figure 3. Map-based cloning of *ZmEHD1*.** (A) Schematic representation of the
797 positional cloning of *ZmEHD1* gene on chromosome 4. The SSR markers, umc1716
798 and umc1650, were used for rough mapping. Recombinants are indicated in
799 parentheses below each SSR marker. (B) Gene structure of *ZmEHD1*. Black boxes
800 indicate exons, and lines between black boxes represent introns. The positions of
801 mutations were marked. The mutations that lead to the amino acid change between the
802 *ehd1* mutant and the WT are indicated with red letters. (C) Schematic representation
803 of the predicted structure of ZmEHD1. The regions encoding the potential protein
804 domains are shown. The positions of mutations on coil-coil domain were marked by
805 asterisks. (D) Real-time RT-PCR detection of *ZmEHD1* gene transcripts in

endosperms of the WT maize and the *ehd1* mutant at 15, 20, 25, and 30 DAP. Quantifications were normalized to the expression of 18S rRNA. Values are means and standard errors (n=3). ** indicates a significant difference ($P < 0.01$) between the WT and the *ehd1* mutant.

Figure 4. Transgenic validation of *ZmEHD1*. (A) Germination of inbred line ZZC01 (WT) and *ZmEHD1* knock-out mutants (KO). Values are means and standard errors of approximately 100 seeds from three independent experiments. An LSD test was used to assess differences between WT and *ZmEHD1* knock-out mutant. **, $P < 0.01$ (t-test), significant difference between WT and KO mutants. (B) Phenotypes of WT and KO mutants (n=20). Representative photograph is shown. (C) Heterozygous *KO*(+/-) × *ehd1*(+/-) were used in an allelism test. The red arrows indicated the *ehd1* kernels. (D) The mature kernels of WT and *KO/ehd1* mutant randomly selected from ears of *KO*(+/-) × *ehd1*(+/-). Scale bars = 0.5 cm. (E) Germination of WT and *KO/ehd1* mutant. Values are means and standard errors of approximately 140 seeds from three independent experiments. An LSD test was used to assess differences between WT and *KO/ehd1* mutant. **, $P < 0.01$ (t-test), significant difference between WT and *KO/ehd1* mutant.

Figure 5. Endocytosis of FM4-64 is reduced in the *ehd1* and in *ZmEHD1* knock-out mutants. Three dimensional reconstructions of z-stacks (60 μM with 2.4-μM steps) were obtained in the *ehd1* (A) and in *ZmEHD1* knock-out mutant (B). FM-64 labeled BFA bodies in the *ehd1* mutant (C) and in *ZmEHD1* knock-out mutants (D). Representative photographs at indicated durations are shown. Scale bars = 10 μm. Numbers below the photographs indicate the rate of FM4-64-labelled fluorescent puncta (% and number of FM4-64-labelled fluorescent puncta/total cell number). ** indicates a significant difference from the WT at $P < 0.01$ according to a *t*-test.

Figure 6. ZmEHD1 directly interacts with the ZmAP2 σ subunit in plants and

836 **yeast.** (A) Interaction between ZmEHD1 and the ZmAP2 σ subunit in the leaves of *N.*
837 *benthamiana*as observed by BiFC. The photographs were taken in the dark field for
838 yellow fluorescence. Propidium iodide (PI) was used to determine the vitality of the
839 cells. Representative photographs are shown. Scale bars = 10 μm. (B) Interaction
840 between ZmEHD1 and the ZmAP2 σ subunit as indicated by split-ubiquitin yeast
841 two-hybrid assays. The ZmAP2 σ subunit was used as the fused bait protein (AP2
842 σ-Cub), and ZmEHD1 was used as the fused prey protein (NubG-ZmEHD1). The
843 presence or absence of His or X-Gal is indicated. (C) Pull-down assays for the
844 interaction between ZmEHD1 and the ZmAP2 σ subunit. The ZmEHD1/ $ZmEHD1_{mut}$
845 in the pull-downed fraction was detected by immunoblot using anti-His antibody.
846
847 **Figure 7. Auxin distribution and ZmPIN1a-YFP localization were altered in the**
848 ***ehd1* mutant.** (A) The response of horizontally placed mesocotyl-coleoptiles to
849 gravity is delayed in *ehd1* mutant (n=15). (B) Free IAA contents in WT maize and
850 *ehd1* mutant kernels at 15 DAP. Error bars represent standard errors (n=4). ** indicates
851 a significant difference from the WT at $P < 0.01$ according to a *t*-test. (C) The
852 fluorescence of ZmDR5::mRFP in WT and *ehd1* mutant. Scale bars = 50 μm. (D) The
853 fluorescence of ZmPIN1a::YFP in WT and *ehd1* mutant. Scale bars = 50 μm. cc,
854 central cylinder; me, root meristem; rc, root cap; co, cortex.
855
856 **Figure 8. Rescue of the *ehd1* phenotype by exogenous 1-NAA.** (A) Germination of
857 the *ehd1* mutant *ZmEHD1* knock-out mutants (KO) after treatment with water alone
858 or with different concentrations of 1-NAA. Values are means and standard errors of
859 approximately 100 seeds from three independent experiments. An LSD test was used
860 to assess differences between treatments. Means with the same letter are not
861 significantly different at $P < 0.01$. (B) Phenotypes of *ehd1* and KO seedlings treated
862 with different concentrations of 1-NAA.
863
864 **Supplemental Table 1. The ear performance of F_2 and F_3 individuals evaluated in**
865 **the fields.**

Supplemental Table 2. The kernel performance of F_2 population evaluated in the fields.

Supplemental Table 3. Oligos used as primers in the experiment.

Supplemental Table 4. Allelism test between *KO*+/- and *ehd1*+/-

Supplemental Table 5. List of genes with significant expression changes.

Supplemental Figure 1. The alignment with AtEHD1, AtEHD2, ZmEHD1 and $ZmEHD_{mut}$. The motifs are underlined.

Supplemental Figure 2. Tissue pattern of *ZmEHD1* transcript accumulation.

Supplemental Figure 3. The observed target deletion of *ZmEHD1* in *ZmEHD1* loss-of-function mutants.

Supplemental Figure 4. The different subcellular localization of ZmEHD1 protein (A) and $ZmEHD1_{mut}$ protein (B). Representative photographs are shown.

Supplemental Figure 5. Rescue of *Arabidopsis ap2 σ* mutant by the *ZmAP2 σ* cDNA. (A) Identification of *ap2 σ* T-DNA insertion mutant. (B) Semi-quantitative RT-PCR analysis of *ZmAP2 σ* transcript levels in the Col, *ap2 σ* mutant and *35S::ZmAP2 σ* transgenic plants. (C) Three week-old and five week-old of WT (left), *ap2 σ* mutant (middle) and *35S::ZmAP2 σ* transgenic plants.

Supplemental Figure 6. Interaction between ZmEHD1 and the ZmAP2 σ subunit in maize mesophyll protoplasts observed by BiFC. The photographs were taken in the dark field for yellow fluorescence. Representative photographs are shown. Scale bars = 10 μm.

Supplemental Figure 7. The different subcellular localization of ZmAP2 σ subunit in WT maize and *ehd1* mutant. Representative photographs are shown. Scale bars = 10 μm.

Supplemental Figure 8. Pearson's correlation coefficients (*R* value) of biological replicates in the WT maize and the *ehd1* mutant.

Supplemental Figure 9. Validation of RNA-Seq by real-time RT-PCR. (A) Genes listed in Supplemental Table 5. (B) Genes listed in Table 1.

Supplemental Figure 10. Germination of the *ehd1* mutant (A) and *ZmEHD1* knock-out mutant (B) treated with water alone or with different concentrations of GA3. Values are means and standard errors of approximately 150 seeds from three independent experiments.

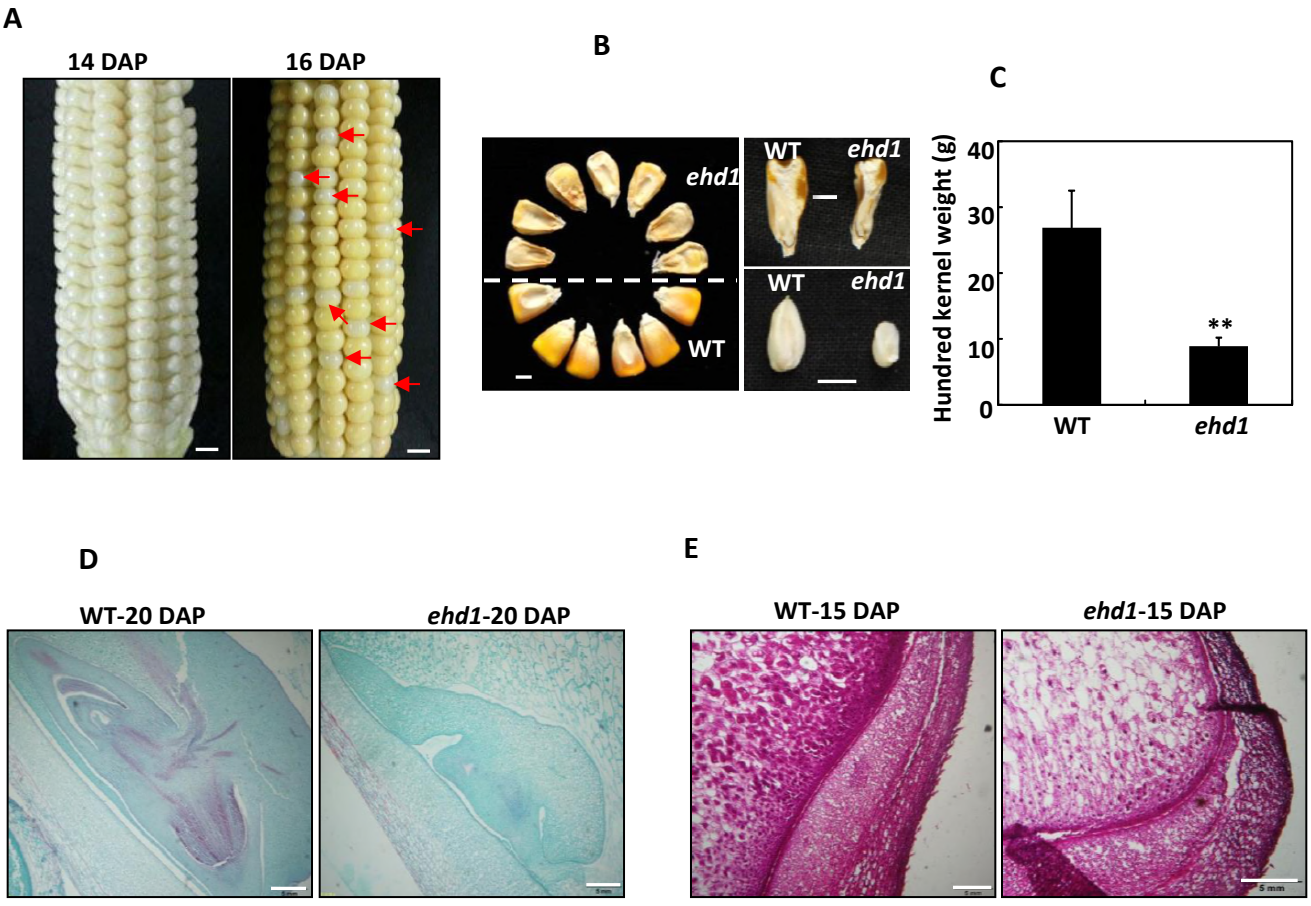

Figure 1. Phenotypes of the maize *ehd1* mutant kernels. (A) F_2 ears of *ehd1* × Xun9058 at 14 or 16 days after pollination (DAP). The red arrows indicated the *ehd1* kernels. Scale bars = 1 cm. (B) The mature kernels of wild type (WT) and *ehd1* mutant randomly selected from F_2 ears of *ehd1* × Xun9058. Scale bars = 0.5 cm. (C) 100-grain weight of the WT and the *ehd1* mutant. Values are means and standard errors (n=4). ** indicates a significant difference ($P < 0.01$) between the WT and the *ehd1* mutant. (D) Comparison of WT and *ehd1* embryos at 20 DAP. The sections stained with Safranin and Fast Green. Scale bars = 5 mm. (E) Microstructure of WT and *ehd1* endosperms at 15 DAP. The sections stained with fuchsin. Scale bars = 5 mm.

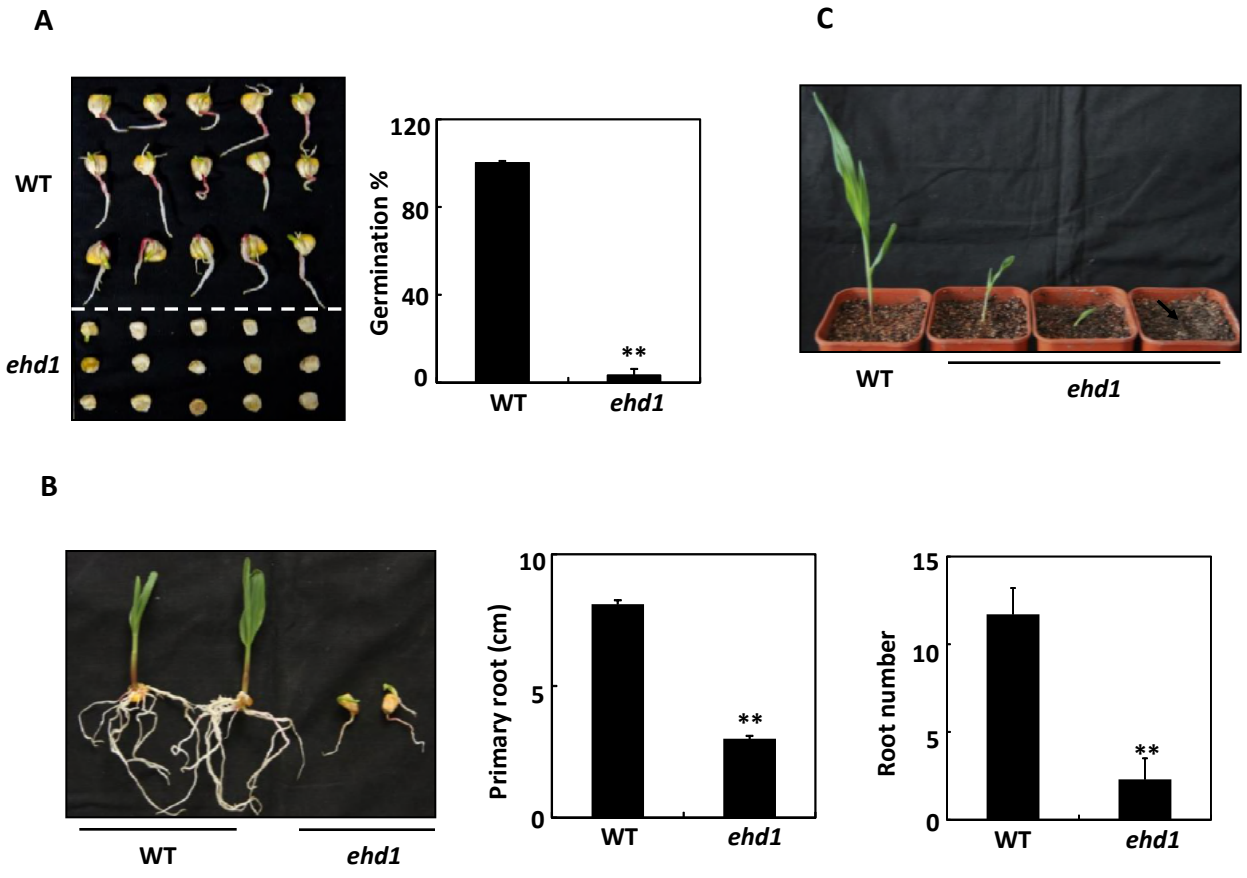

Fig. 2 *ZmEHD1* is required for normal growth and development of maize. (A) Germination of the WT and the *ehd1* mutant. Values are means and standard errors of approximately 100 seeds from three independent experiments. (B) Root number and root elongation of the WT and the *ehd1* mutant. Values are means and standard errors (n=5). ** indicates a significant difference ($P < 0.01$) between the WT and the *ehd1* mutant. (C) Phenotypes of WT and *ehd1* seedlings (n=30). Representative photograph is shown.

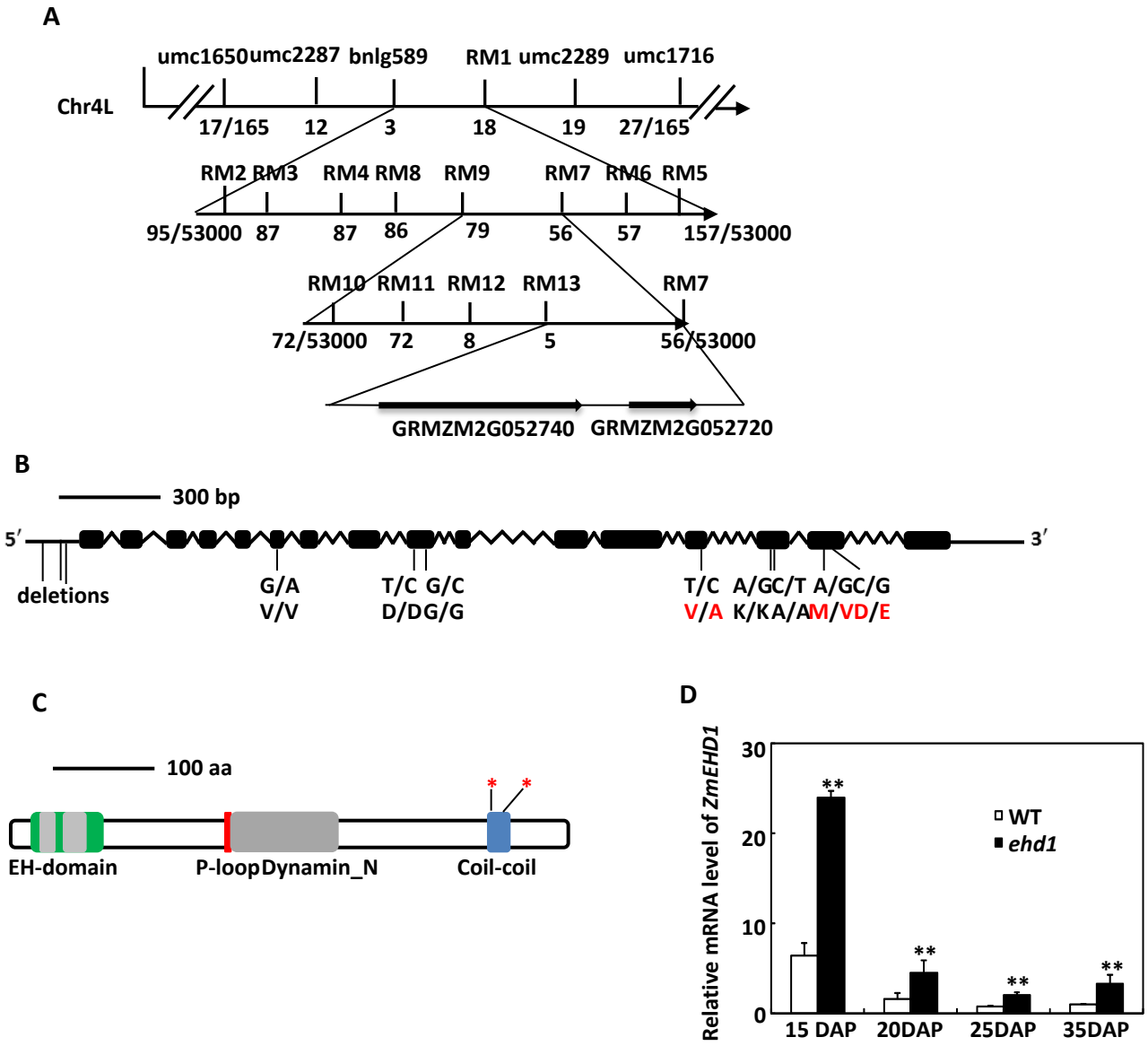

Fig. 3 Map-based cloning of *ZmEHD1*. (A) Schematic representation of the positional cloning of *ZmEHD1* gene on chromosome 4. The SSR markers, umc1716 and umc1650, were used for rough mapping. Recombinants are indicated in parentheses below each SSR marker. (B) Gene structure of *ZmEHD1*. Black boxes indicate exons, and lines between black boxes represent introns. The positions of mutations were marked. The mutations that lead to the amino acid change between the *ehd1* mutant and the WT are indicated with red letters. (C) Schematic representation of the predicted structure of ZmEHD1. The regions encoding the potential protein domains are shown. The positions of mutations on coil-coil domain were marked by asterisks. (D) Real-time RT-PCR detection of *ZmEHD1* gene transcripts in endosperms of the WT maize and the *ehd1* mutant at 15, 20, 25, and 30 DAP. Quantifications were normalized to the expression of 18S rRNA. Values are means and standard errors (n=3). ** indicates a significant difference ($P < 0.01$) between the WT and the *ehd1* mutant.

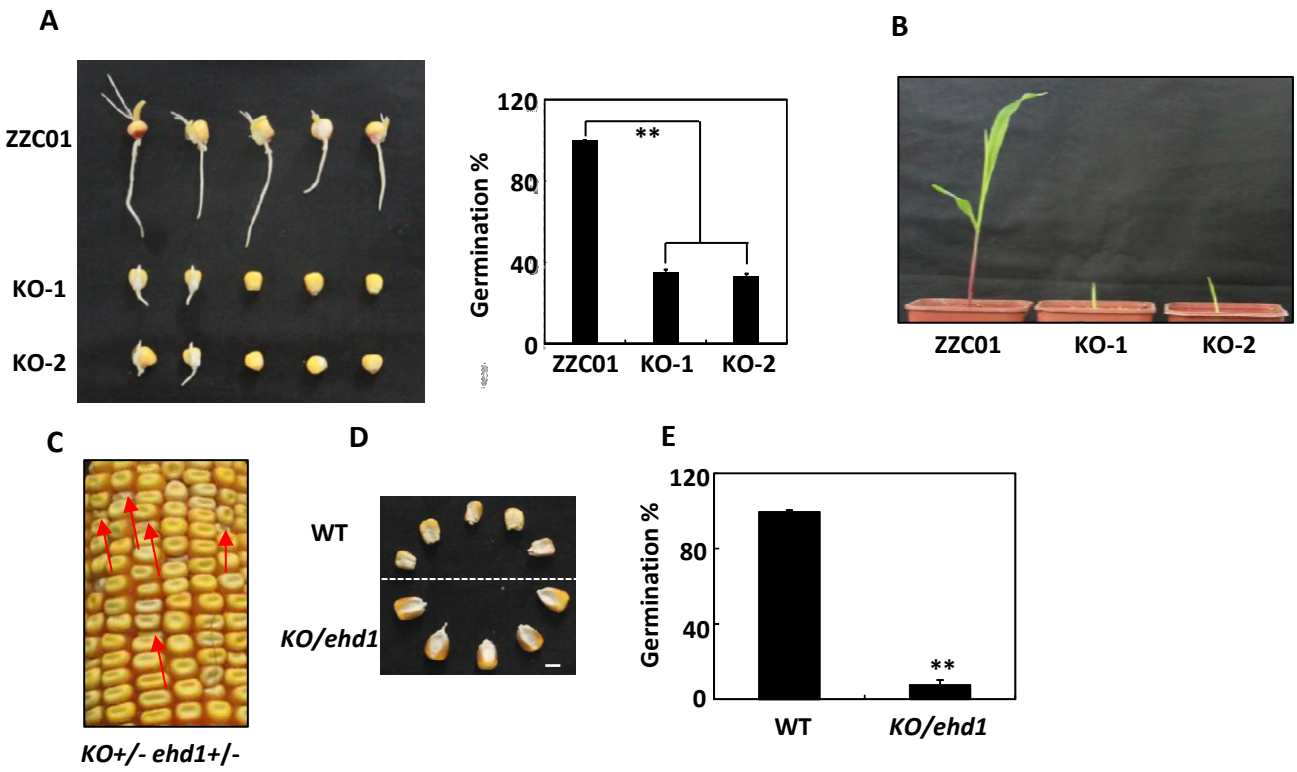

Fig. 4 Transgenic validation of *ZmEHD1*. (A) Germination of inbred line ZZC01 (WT) and *ZmEHD1* knock-out mutants (KO). Values are means and standard errors of approximately 100 seeds from three independent experiments. An LSD test was used to assess differences between WT and *ZmEHD1* knock-out mutant. **, P < 0.01 (t-test), significant difference between WT and KO mutants. (B) Phenotypes of WT and KO mutants (n=20). Representative photograph is shown. (C) Heterozygous *KO*(+/-) × *ehd1*(+/-) were used in an allelism test. The red arrows indicated the *ehd1* kernels. (D) The mature kernels of WT and *KO/ehd1* mutant randomly selected from ears of *KO*(+/-) × *ehd1*(+/-). Scale bars = 0.5 cm. (E) Germination of WT and *KO/ehd1* mutant. Values are means and standard errors of approximately 140 seeds from three independent experiments. An LSD test was used to assess differences between WT and *KO/ehd1* mutant. **, P < 0.01 (t-test), significant difference between WT and *KO/ehd1* mutant.

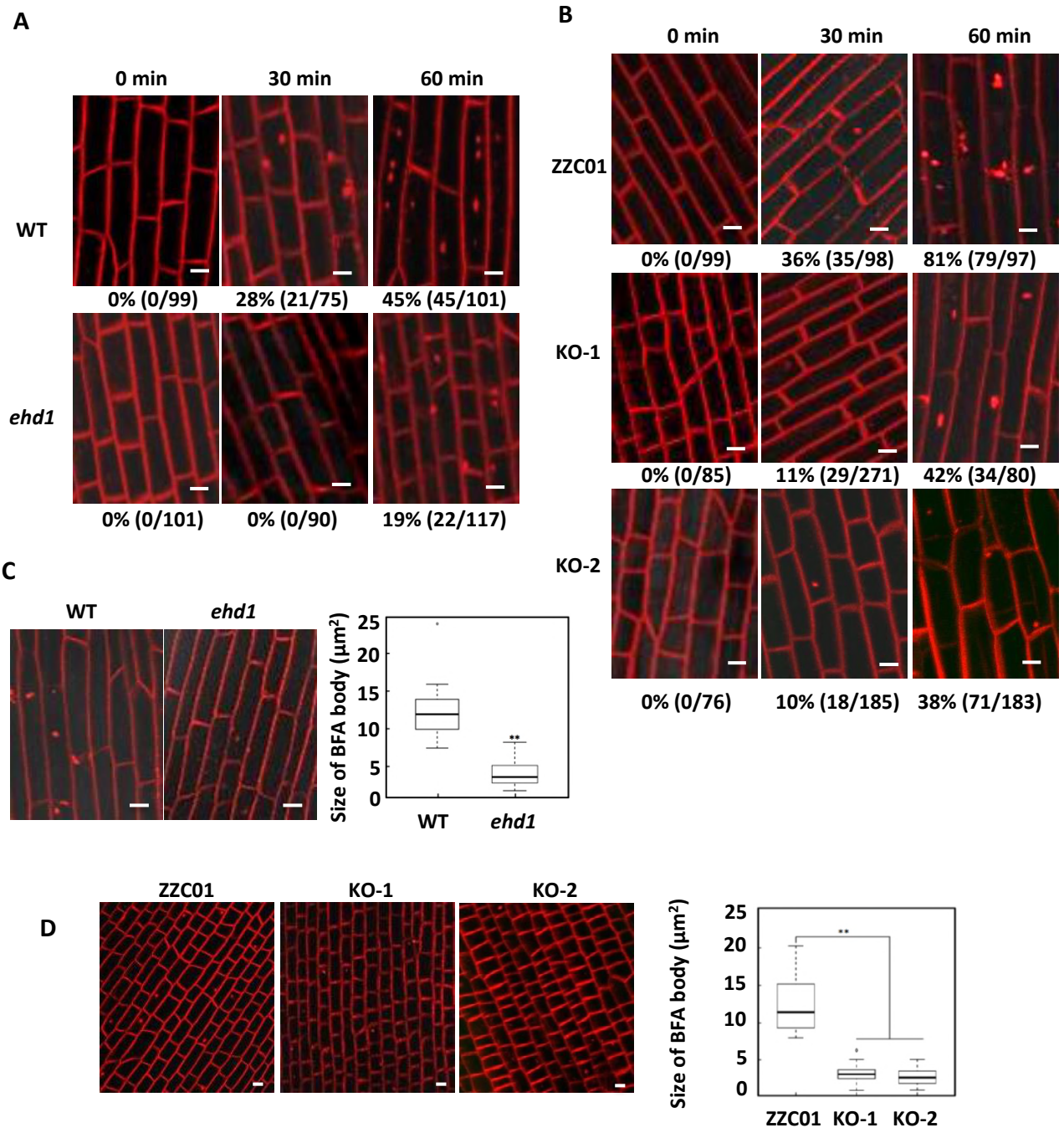

Fig. 5 Endocytosis of FM4-64 is reduced in the *ehd1* and in *ZmEHD1* knock-out mutants. Three dimensional reconstructions of z-stacks (60 μM with 2.4-μM steps) were obtained in the *ehd1* (A) and in *ZmEHD1* knock-out mutant (B). FM-64 labeled BFA bodies in the *ehd1* mutant (C) and in *ZmEHD1* knock-out mutants (D). Representative photographs at indicated durations are shown. Scale bars = 10 μm. Numbers below the photographs indicate the rate of FM4-64-labelled fluorescent puncta (% and number of FM4-64-labelled fluorescent puncta/total cell number). ** indicates a significant difference from the WT at $P < 0.01$ according to a *t*-test.

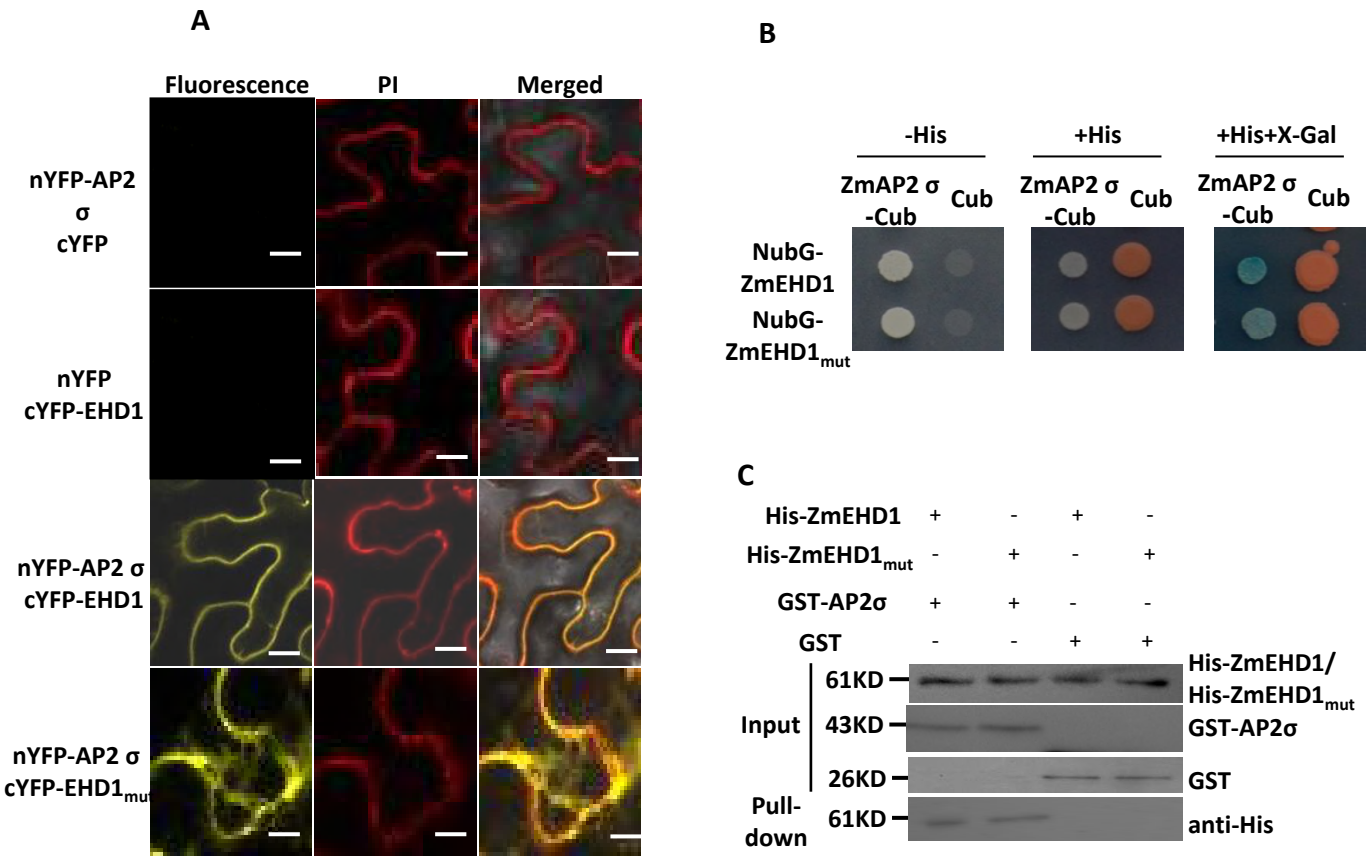

Figure 6. ZmEHD1 directly interacts with the ZmAP2 σ subunit in plants and yeast. (A) Interaction between ZmEHD1 and the ZmAP2 σ subunit in the leaves of *N. benthamiana*as observed by BiFC. The photographs were taken in the dark field for yellow fluorescence. Propidium iodide (PI) was used to determine the vitality of the cells. Representative photographs are shown. Scale bars = 10 μm. (B) Interaction between ZmEHD1 and the ZmAP2 σ subunit as indicated by split-ubiquitin yeast two-hybrid assays. The ZmAP2 σ subunit was used as the fused bait protein (AP2 σ-Cub), and ZmEHD1 was used as the fused prey protein (NubG-ZmEHD1). The presence or absence of His or X-Gal is indicated. (C) Pull-down assays for the interaction between ZmEHD1 and the ZmAP2 σ subunit. The ZmEHD1/ $ZmEHD1_{mut}$ in the pull-downed fraction was detected by immunoblot using anti-His antibody.

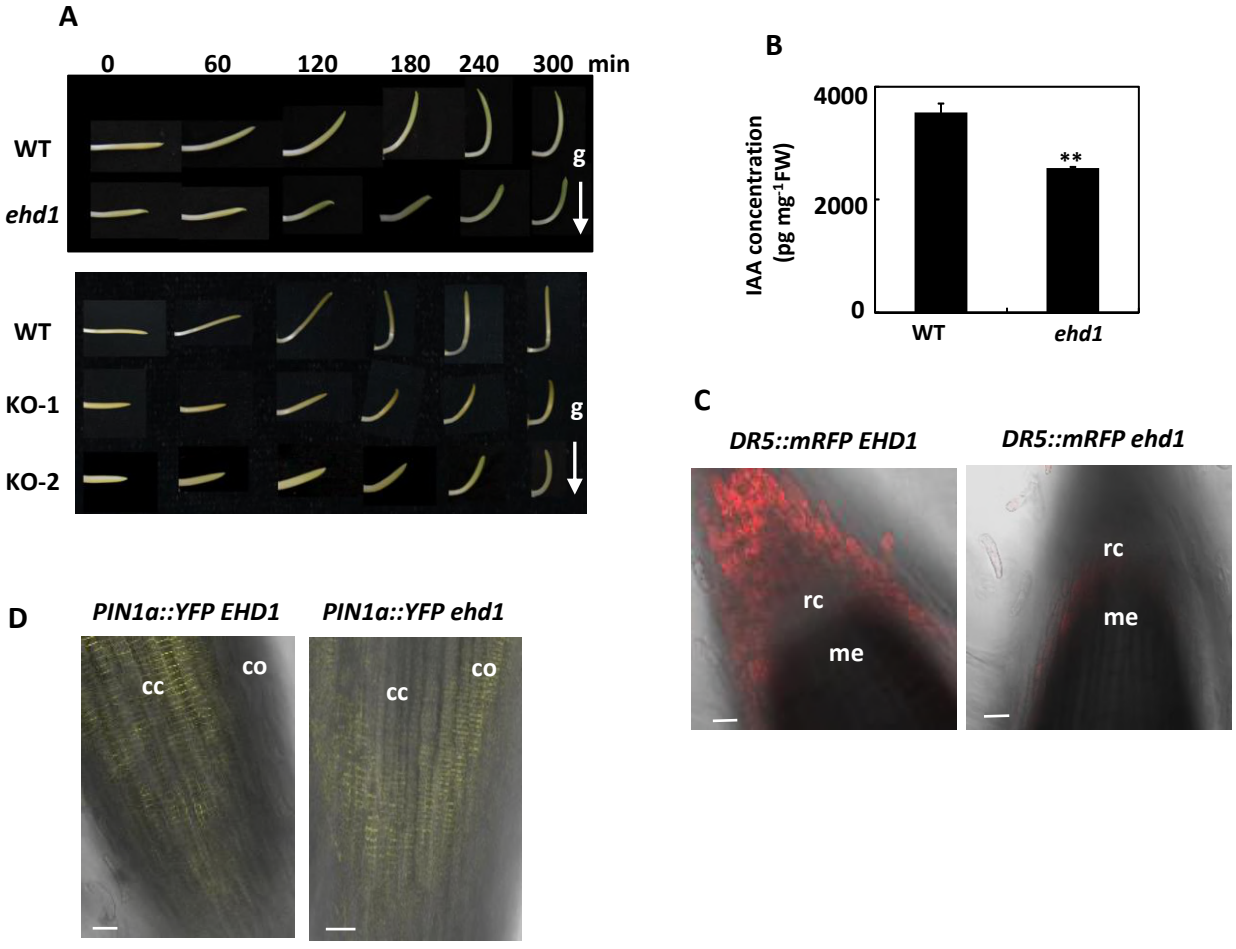

Figure 7. Auxin distribution and ZmPIN1a-YFP localization were altered in the *ehd1* mutant. (A) The response of horizontally placed mesocotyl-coleoptiles to gravity is delayed in *ehd1* mutant (n=15). (B) Free IAA contents in WT maize and *ehd1* mutant kernels at 15 DAP. Error bars represent standard errors (n=4). ** indicates a significant difference from the WT at $P < 0.01$ according to a *t*-test. (C) The fluorescence of ZmDR5::mRFP in WT and *ehd1* mutant. Scale bars = 50 µm. (D) The fluorescence of ZmPIN1a::YFP in WT and *ehd1* mutant. Scale bars = 50 µm. cc, central cylinder; me, root meristem; rc, root cap; co, cortex.

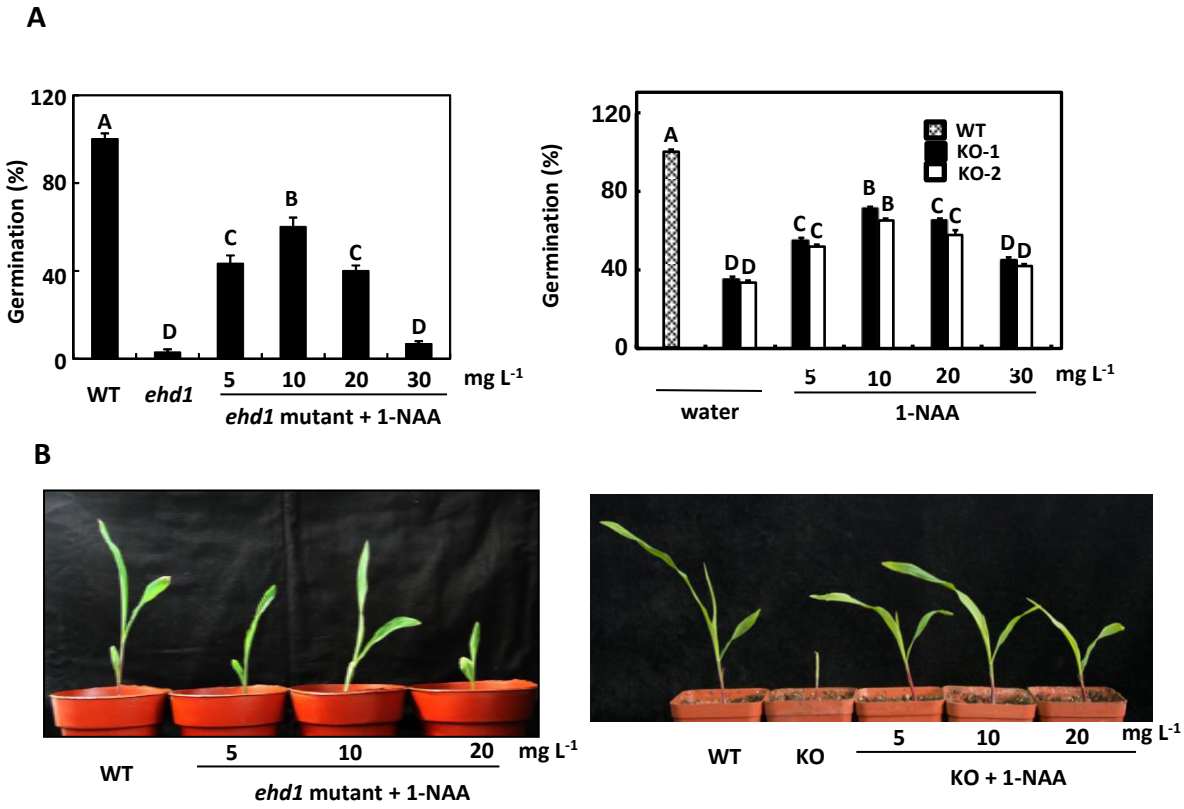

Figure 8. Rescue of the *ehd1* phenotype by exogenous 1-NAA. (A) Germination of the *ehd1* mutant *ZmEHD1* knock-out mutants (KO) after treatment with water alone or with different concentrations of 1-NAA. Values are means and standard errors of approximately 100 seeds from three independent experiments. An LSD test was used to assess differences between treatments. Means with the same letter are not significantly different at $P < 0.01$. (B) Phenotypes of *ehd1* and KO seedlings treated with different concentrations of 1-NAA.